

High Temporal Resolution Functional MRI Using Parallel Echo Volumar Imaging

Cécile Rabrait, MS,^{1*} Philippe Ciuciu, PhD,¹ Alejandro Ribés, PhD,¹ Cyril Poupon, PhD,¹ Patrick Le Roux, PhD,² Ghislaine Dehaine-Lambertz, MD, PhD,^{1,3} D. Le Bihan, MD, PhD,¹ and F. Lethimonnier, PhD¹

Purpose: To combine parallel imaging with 3D single-shot acquisition (echo volumar imaging, EVI) in order to acquire high temporal resolution volumar functional MRI (fMRI) data.

Materials and Methods: An improved EVI sequence was associated with parallel acquisition and field of view reduction in order to acquire a large brain volume in 200 msec. Temporal stability and functional sensitivity were increased through optimization of all imaging parameters and Tikhonov regularization of parallel reconstruction. Two human volunteers were scanned with parallel EVI in a 1.5T whole-body MR system, while submitted to a slow event-related auditory paradigm.

Results: Thanks to parallel acquisition, the EVI volumes display a low level of geometric distortions and signal losses. After removal of low-frequency drifts and physiological artifacts, activations were detected in the temporal lobes of both volunteers and voxelwise hemodynamic response functions (HRF) could be computed. On these HRF different habituation behaviors in response to sentence repetition could be identified.

Conclusion: This work demonstrates the feasibility of high temporal resolution 3D fMRI with parallel EVI. Combined with advanced estimation tools, this acquisition method should prove useful to measure neural activity timing differences or study the nonlinearities and nonstationarities of the BOLD response.

Key Words: echo volumar imaging; parallel MRI; SENSE; fMRI; high temporal resolution

J. Magn. Reson. Imaging 2008;27:744–753.

© 2008 Wiley-Liss, Inc.

acquisition of multislice brain volumes with a spatial resolution of about 3 mm and a temporal resolution of 1–2 seconds. EPI is thus well suited to the detection of cerebral activations and the mapping of activated areas. Nevertheless, with the development of event-related fMRI (1) and the growing interest in the temporal features of the hemodynamic response function (HRF) (2,3), higher scanning rates are called for by neuroscientists.

High temporal resolution fMRI is feasible with echo volumar imaging (EVI), a 3D extension of EPI, in which a 3D Fourier space is encoded in a single-shot acquisition. Some applications of EVI have been reported, especially in fMRI (4–6). As compared with EPI, EVI presents several advantages for fMRI. First, EVI acquisition offers very short TR, on the order of 200 msec. Second, 3D single-shot acquisition makes slice-timing correction unnecessary and reduces the risk of intravolume motion of the subject. Finally, true 3D acquisition is known to reduce vascular inflow effects (7) that often confuse the interpretation of fMRI results (8).

Nevertheless, EVI has seldom been used in fMRI, due to its heavy demand on gradient hardware. Actually, because of hardware limitations the echo train duration (ETD) is high in EVI and the voxel bandwidth along the direction of partition (third encoding direction) is very low. Thus, if high spatial resolution and wide brain coverage are required in an EVI acquisition, susceptibility-induced distortions and signal losses due to T2* relaxation dramatically alter image quality. To overcome these difficulties compromises between acquisition time and spatial parameters must be found. Previously reported EVI studies have preferentially used the frequency encoding direction (less expensive in acquisition time) and acquired highly anisotropic volumes. However, this geometry is not suitable to every fMRI experiment and, because of the small number of samples along the partition direction, the Fourier transform is not a reliable estimator of the object's real spin density.

In this context, our purpose was to develop an EVI method allowing single-shot acquisition of a nearly isotropic volume covering most of the human brain. It was achieved, for the first time, by combining EVI with parallel acquisition and SENSE reconstruction, along both

UNTIL NOW, functional MRI (fMRI) data were mostly acquired using echo planar imaging (EPI), allowing the

¹CEA/DSV/I²BM/Neurospin, Gif-sur-Yvette, France.

²GEHC, Buc, France.

³Unité INSERM 562, Gif-sur-Yvette, France.

*Address reprint requests to: C.R., CEA/DSV/I²BM/Neurospin/LRMN, CEA Saclay, Bât. 145, 91191 Gif-sur-Yvette cedex, France.
E-mail: cecile.rabrait@ambre.net

Received July 4, 2007; Accepted January 8, 2008.

DOI 10.1002/jmri.21329

Published online in Wiley InterScience (www.interscience.wiley.com).

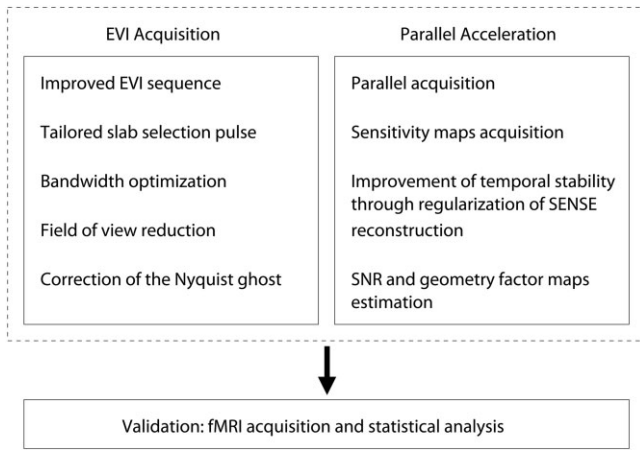


Figure 1. Schematic diagram illustrating the different steps involved in parallel acquisition of EVI volumes.

the phase and partition directions (9). An acceleration factor of 4 was reached, making it possible to acquire a $120 \times 120 \times 144 \text{ mm}^3$ brain volume in 200 msec. To achieve 3D single-shot acquisition of a large brain volume and keep the level of susceptibility-induced distortions low, the spatial resolution was limited to 6 mm. This spatial scale is commonly used in neuroscience group studies, which involve brain normalization.

In this article the adaptation of 2D-SENSE reconstruction to localized EVI volumes is described. The optimization of all the imaging parameters to maximize the SNR is discussed and the effect of regularization on functional sensitivity is investigated. An auditory, slow event-related functional paradigm is used to demonstrate the feasibility of detecting brain activation and estimating high temporal resolution hemodynamic response functions with parallel EVI.

MATERIALS AND METHODS

To clarify the presentation of the different steps required to achieve parallel EVI, we introduce a schematic diagram describing the whole process in Fig. 1.

EVI Acquisition

In order to prevent the formation of an N/2 ghosting artifact along the partition direction, a modified EVI sequence with rewind gradients was implemented, as previously (6). The area of the rewind gradient, applied along the phase direction after the encoding of each section, exactly compensates for the accumulated area of the phase blipped gradients. Thus, contrary to conventional EVI (10), alternate planes in Fourier space are acquired under phase encoding gradients with the same polarity, as illustrated in Fig. 2.

Slab selective excitation was performed by a spectrospatial radiofrequency (RF) pulse (11), so that subcutaneous fat was not excited. This pulse was composed of eight spatially selective pulses (duration 1.5 msec), with variable magnitudes and separated by 2.27-ms wait periods, as illustrated in Fig. 2. A slab-selection gradient was applied during the RF pulses and magnetiza-

tion was rephased by another gradient during wait periods. The complete pulse lasts 18.2 msec and its bandwidth is equal to 10 kHz. The spatial selectivity of the pulse, defined as the ratio of the pass bandwidth to the transition bandwidth, was high (around 15) and the suppression of the fat signal was efficient. The spatial selectivity of the slab selection pulse was sufficient to define the thickness of the acquired volume along the partition direction.

In order to limit susceptibility-induced distortions and signal losses, the ETD must be minimized. The ETD was estimated as a function of all relevant imaging parameters. It appears that, in parallel EVI with trapezoidal gradient pulses, ramp-sampling acquisition does not allow one to significantly reduce the ETD, mainly because of the rewind gradient and of the small matrices acquired. Hence, it has not been introduced. Moreover, since the frequency encoding gradient amplitude depends on the acquisition bandwidth and because of the limited slew rate of the gradient hardware, there is an optimal readout bandwidth minimizing the ETD, which depends on N_x , N_y , field of view (FOV) along the readout direction, and gradient rise time. The choice of the optimal bandwidth significantly reduces the ETD. For example, for a $20 \times 20 \times 24$ matrix, with a $120 \times 120 \times 144 \text{ mm}^3$ FOV and an acceleration factor of 2 along two directions ($R = 2 \times 2$), the optimal acquisition bandwidth is 100.0 kHz, corresponding to an ETD of 58 msec. Bandwidth of 50 kHz and 200 kHz correspond respectively to ETD of 68 and 74 msec.

To further reduce the ETD the FOV was reduced as proposed previously (5,6). Outer volume suppression (OVS) was applied before excitation in order to avoid wraparound artifacts. Two quadratic phase pulses, designed with the Shinnar-Le Roux algorithm, each of which being followed by spoiler gradient pulses, were applied in conjunction with a slab-selective gradient along the phase direction (12). The quadratic phase pulses (duration: 4 msec, bandwidth: 10 kHz) offer a high spatial selectivity (around 20) and a low peak B_1 . To ensure a good suppression of the external signal, OVS pulses were repeated twice, before each excitation.

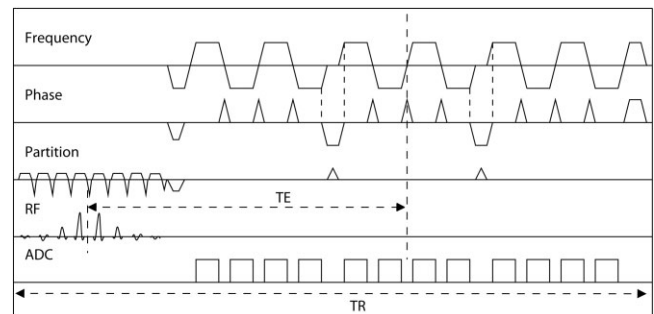


Figure 2. Timing diagram of the EVI sequence: a spectrospatial slab excitation pulse is followed by a modified EVI echo train. In this example only four phase encoding lines and three sections are acquired. For sake of simplicity, the outer volume suppression module is not included on this diagram. This module takes place before excitation and is presented in Ref. (12).

After 3D reconstruction, EVI volumes are affected by a Nyquist $N/2$ ghosting artifact along the phase direction, as in EPI. It is due to small timing differences between odd and even echoes. The well-known calibration scan method (13) was used to correct for these differences. A calibration scan was acquired at the beginning of the functional time series, with neither phase nor partition gradients. Calibration data were first Fourier transformed with respect to the frequency encoding direction. Then, Ahn's coefficients (constant and linear) were computed for every phase encoding step (14) and used to correct all the volumes of the temporal series. Contrary to (13), Ahn's coefficients have not been modeled since discontinuities appeared between k -space sections. Moreover, if the ETD is kept short, Ahn's correction is sufficient to reduce ghosting artifact efficiently in EVI volumes at 1.5T.

Parallel Acceleration

Parallel Acquisition

Minimization of the ETD by choosing the optimal acquisition bandwidth and restricting the FOV does not permit reaching short ETD while covering a large part of the brain. As shown by the previous example ($20 \times 20 \times 24$ matrix, $120 \times 120 \times 144$ mm³ FOV), without parallel acceleration the minimized ETD would be in the 230–240 msec range. The only way to dramatically reduce the ETD is to use parallel imaging in order to undersample k -space acquisition along both the phase and partition directions. In 3D imaging the choice of 2D-SENSE parallel acquisition and reconstruction is advantageous since geometry factors are lower than in 1D-SENSE for a given acceleration factor; the SNR of the reconstructed volumes is thus higher (9). All 2D-SENSE acquisitions were performed in either sagittal or coronal orientations. Indeed, the nearly cylindrical coil we used (8-channel head coil) prohibits SENSE reconstruction along its main axis, since its sensitivity is nearly uniform along this direction. Parallel acquisition also directed the optimization of the imaging parameters. Indeed, the FOV has to be relatively large along both undersampling directions, since parallel reconstruction is easier when the difference of sensitivities between signal components superimposed in a given voxel is more important. Moreover, the additional degrees of freedom offered by parallel imaging (15) allowed reducing acoustic noise through minor parameter tuning. This optimization resulted in a decrease from about 115 dB to an acceptable level of 104 dB.

Parallel Reconstruction: Acquisition of the Sensitivity Maps

Parallel reconstruction of EVI undersampled volumes was performed with an in-house-developed multidimensional SENSE algorithm (16). To perform SENSE reconstruction it was necessary to acquire sensitivity maps for each RF channel. In EVI this step was crucial. It was indeed impossible to use an EVI volume as a sensitivity map, since the high level of geometric distortions and signal losses would make the map useless. EPI images could not be used as sensitivity maps either,

since the distortions are not the same as in parallel EVI. Therefore, conventional 2D gradient echo images were acquired as sensitivity maps. One critical issue was to make sure that distortions remain low in EVI, so that EVI volumes and sensitivity maps could be superimposed. Empirical optimization of the ETD was thus performed by experimenting parallel reconstruction of EVI volumes for a large range of ETD (data not shown). This study led to restricting the ETD below 60 msec, although EPI acquisitions at 1.5T frequently use longer ETD. Full FOV sensitivity maps have been preferred since SNR is higher in full FOV images compared to reduced FOV images. Sensitivity maps were automatically cropped to match the EVI volume after the building of a binary mask of the brain. This mask was used to remove voxels outside of the brain from parallel reconstruction. This "voxel exclusion" operation improved the SNR of the reconstructed volumes (9). Given the low spatial resolution of parallel EVI volumes, the impact of Gibb's ringing artifacts should be considered, as in parallel spectroscopic imaging (17,18). In parallel EVI, as spatial resolution is the same in sensitivity maps and parallel data, Gibb's artifact should be similar. Nevertheless, Gibb's side lobes could be important in parallel data while being excluded from the masked sensitivity maps. To avoid this problem the binary brain mask was dilated by a few voxels as proposed previously (17). Alternatively, a cosine filter could be applied in k -space, which apodizes the reconstructed data while degrading the spatial resolution. A more efficient solution, which improves SENSE reconstruction by taking into account the real point spread function, has also been proposed (18).

As explained previously (19), noise properties should be obtained from artifact-free data, preferably from noise-only samples. In the present study noise properties were estimated from an empty area in the sensitivity maps to reduce the total acquisition duration and because 2D gradient echo is not very sensitive to image artifacts. Gibb's artifact, which is the more likely to occur, should have a small effect since noise properties are estimated outside of the dilated mask.

Parallel Reconstruction: Regularization

Typically, regularization techniques are used in parallel reconstruction to improve the visual quality of static images. Nevertheless, since parallel EVI aims at detecting cerebral activations, temporal signal stability is a predominant criterion over image quality. In the present work, as pioneered previously (20,21), regularization of parallel reconstruction was used to improve signal stability and activation detection. Tikhonov weighting (22) was applied, with a regularization condition minimizing the magnitude of the MR signal in reconstructed volumes, as before (23). The relative importance of the regularization term was modulated by a regularization parameter, λ^2 , empirically set.

To investigate the impact of regularization, SNR maps, geometry factor maps, and statistical scores were computed for increasing values of λ^2 . These values range from 10^{-4} to 0.2. At $\lambda^2 = 10^{-4}$, reconstructed volumes are highly similar to volumes reconstructed

without regularization, while avoiding computer errors due to small singular values. At $\lambda^2 = 0.2$ statistical scores have reached a plateau, while reconstruction artifacts become important. The number of intermediate settings was kept small because of the strong efforts required to perform the statistical analysis for each setting.

To assess signal stability the SNR was defined in each voxel as the ratio of the average signal over its standard deviation in the voxel time course. This definition, often used in cerebral functional imaging (24,25), is reliable when used with parallel imaging. We note that due to the inhomogeneous spatial distribution of the noise other SNR definitions suffer from serious bias (26). SNR measurements were performed after removal of low-frequency drifts and filtering out of physiological artifacts, as described in the next section. The quality of parallel reconstruction was also assessed through the computation of spatial maps of the geometry factor, g , (16). These maps quantify the difficulty to separate the different signal components superimposed in a given voxel. The g factor depends on the geometry of the acquired volume and the coil array.

Data Acquisition and Analysis

Two right-handed healthy male adults were scanned using a Signa 1.5T Excite II MR system (General Electric Healthcare, Milwaukee, WI), employing a gradient coil with a maximum amplitude of $40 \text{ mT}\cdot\text{m}^{-1}$ and a $266\text{-}\mu\text{s}$ minimum rise time. An 8-channel high resolution brain array by MRI Devices was used for parallel acquisition. Acquisitions on human volunteers were approved by a local ethics committee and the subjects gave written informed consent.

For the acquisition of parallel EVI time series the imaging parameters were set as follows: $20 \times 20 \times 24$ matrix, TE/TR = 40/200 msec, 3D-FOV = $120 \times 120 \times 144 \text{ mm}^3$, BW = 100 kHz, flip angle = 35° . The volumes were acquired in sagittal orientation, with the frequency encoding gradient applied in the superior-inferior direction, and the partition encoding gradient applied in the mediolateral direction. A total parallel reduction factor of 4 was applied, corresponding to a reduction factor of 2 along both phase and partition directions. The ETD was equal to 58 msec, while typical ETD in EPI ranged from 30–80 msec on this scanner. The volume of interest had been optimized for auditory paradigms and included the two temporal lobes of an “average” subject. Moreover, the chosen geometry minimizes vascular artifacts due to inflow of venous blood, because of 3D acquisition and low excitation flip angle (7), and since no “fresh” blood can enter the excited volume along the partition direction.

For SENSE parallel reconstruction, 2D gradient-echo sensitivity maps were acquired in sagittal orientation. Acquisition parameters were set as follows: 40×40 matrix, 24 slices, slice thickness = 6 mm, TE/TR = 10/500 msec, FOV = $240 \times 240 \text{ mm}^2$, BW = 62.5 kHz, flip angle = 30° . A high-resolution T1-weighted 3D volume was acquired for anatomical localization ($256 \times 256 \times 128$ matrix, voxel size = $0.9 \times 0.9 \times 1.2 \text{ mm}^3$).

The fMRI paradigm used to validate the detection of cerebral activation consisted in a slow-event presentation of auditory sentences, one short sentence (2200 msec on average) every 14.4 seconds. Each sentence was repeated four times in a row, in order to induce habituation effects as in Ref. (27). Each run comprised 12 different sentences for a total duration of 11 minutes, 41 seconds. The first sentence was preceded by a 9.6-second rest period, corresponding to 48 dummy scans. One run was acquired in each participant.

Postprocessing and statistical analysis of the EVI temporal series were conducted using the SPM2 software (www.fil.ion.ucl.ac.uk). Illustrations were created using the Anatomist software (<http://brainvisa.info>). First, EVI volumes were rotated to match the axial orientation of anatomical data. Second, reconstructed time series were realigned to an EVI volume devoid of artifacts, using a six-parameter linear transformation, and resliced. Third, a numerical band-rejection filter was applied to reduce cardiac (0.8–1.2 Hz) and respiratory artifacts (0.15–0.3 Hz), as in Ref. (6). Physiological artifacts are easily filtered out in EVI thanks to the high sampling frequency. Finally, the volumes were spatially smoothed, using a 10-mm isotropic Gaussian filter. This operation is generally applied to EPI data to assure the accuracy of the statistical inference made from the data in SPM and increase the sensitivity of detection in group studies. It also increases the SNR and thus the sensitivity of detection of brain activations. Rigid coregistration to anatomical data was performed using the Brainvisa software (<http://brainvisa.info>). Since the EVI volume is relatively large, computation of the coregistration parameters was straightforward and accurate. The removing of low-frequency drifts was performed through modeling of the trend by a basis of discrete cosine functions (28) with a 32-second cutoff period.

A generalized linear model was generated by entering four distinct variables corresponding to the four repetition positions of a sentence. The variables, convolved with the standard SPM HRF and its temporal derivative were included in the model. The significance of the activations in response to the first presentation of each sentence was assessed using Student's t -test corrected for multiple comparisons (family-wise error) and thresholded at 10^{-4} .

RESULTS

Image Quality and SNR

As illustrated in Fig. 3, parallel imaging improves EVI image quality, as demonstrated for single-shot acquisition methods (19,29). A spherical water phantom was scanned and EVI volumes were acquired, either with no parallel acceleration or with a reduction factor of 4. In the latter case, undersampling was applied along both phase ($R_y = 2$) and partition ($R_z = 2$) directions. Parallel acquisition results in a decrease of the ETD by a factor of 4, therefore reducing susceptibility-induced distortions and signal dropout. For comparison, reference images (sum of squares of the sensitivity maps) are also displayed, as well as the folded EVI volume (sum of

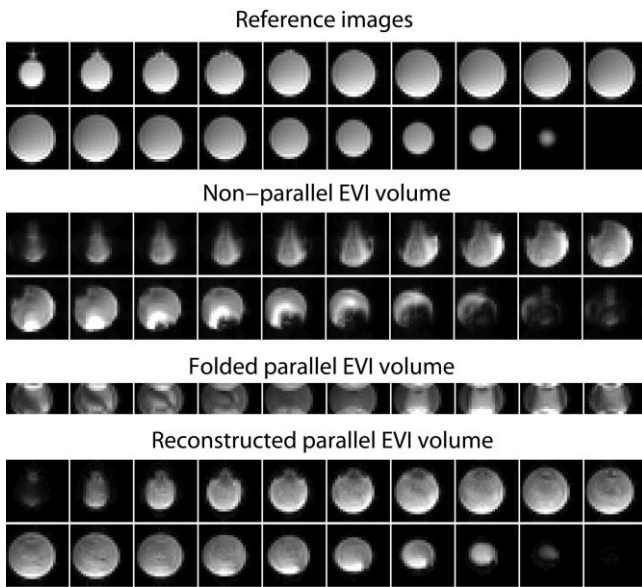


Figure 3. Comparison between nonparallel and parallel EVI volumes. The parallel EVI volume has been acquired with a total parallel acceleration factor of 4. 2D gradient-echo images acquired with the same FOV are displayed as reference. Acquisition parameters: nonparallel EVI volume: $N_x = N_y = 24$, $N_z = 20$, $L_x = L_y = 160$ mm, $L_z = 120$ mm, TE/TR = 116/252 msec, ETD = 216 msec, BW = 125 kHz, flip angle = 35°; parallel EVI volume: $N_x = 24$, $N_y = 12$, $N_z = 10$, $L_x = L_y = 160$ mm, $L_z = 120$ mm, TE/TR = 40/200 msec, ETD = 54 msec, BW = 125 kHz, flip angle = 35°; 2D gradient-echo images: $N_x = N_y = 24$, 20 slices, $L_x = L_y = 160$ mm, slice thickness = 6 mm, TE/TR = 10/500 msec, BW = 62.5 kHz, flip angle = 30°.

squares of the folded volumes reconstructed from the undersampled data). The latter comprises one phase-encoding line over two and one section over two. The reconstructed parallel EVI volume is relatively homogenous and appears highly similar to the reference images, although the TE (40 msec) is longer than the TE used in the acquisition of reference images (10 msec). This similarity can be partially explained by the application of a mask computed from sensitivity data. Nevertheless, the folded EVI volume, which has not been masked, also displays reduced distortions and better signal homogeneity compared to the nonparallel EVI volume.

The 1000th volume extracted from a parallel EVI temporal series acquired on a subject is shown in Fig. 4. This volume was acquired after the magnetization reached a steady state, and is thus representative of the volumes studied for activation detection. In these volumes the signal is relatively homogenous. The only area of low signal corresponds to the lateral ventricles, filled with cerebral spinal fluid (CSF), which presents a lower steady-state signal than gray and white matter at short TR. The homogeneity of the signal along the partition direction validates the good quality of the slab selection pulse. The slight signal diminution in the middle of the volume can be explained by the so-called “SENSE ghost” (30) which comes from residual signal in the external areas. The small amplitude of this effect as-

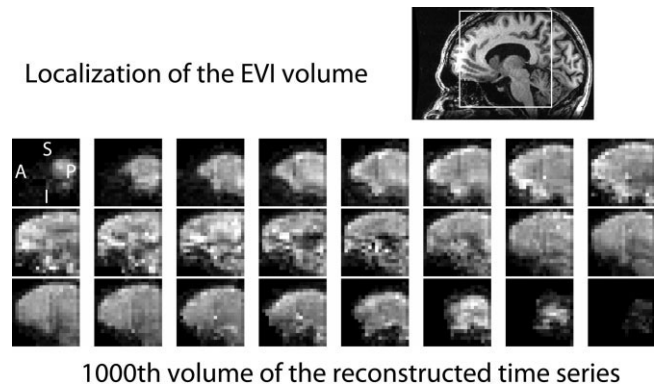


Figure 4. Parallel EVI volume acquired on a human subject and its localization over one slice of the subject's anatomical data. The 1000th volume of the time series is presented, since it is representative of the volumes studied for activation detection. The sections are presented from right to left of the subject's head. Acquisition parameters for the parallel EVI time series: $N_x = 20$, $N_y = 10$, $N_z = 12$, $L_x = L_y = 120$ mm, $L_z = 144$ mm, TE/TR = 40/200 msec, ETD = 58 msec, BW = 100 kHz, flip angle = 35°, regularization parameter (λ^2) = 10^{-2} .

sesses the high level of signal suppression achieved. In 3D sagittal acquisitions, distortions could occur along the phase (A/P) and partition (R/L) directions. The low level of distortions is illustrated in Fig. 5, showing the superimposition of a parallel EVI volume over anatomical images, displayed as a set of (R/L, A/P) planes. Accurate coregistration between parallel EVI data and anatomical data is observed, as required for correct localization of cerebral activations.

SNR maps were computed after filtering out cardiac and respiratory artifacts. Before filtering, signal values

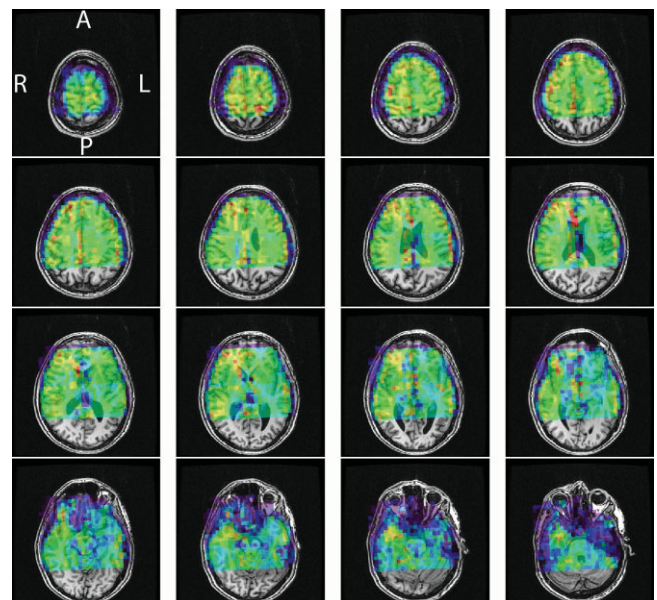


Figure 5. Superimposition of the EVI volume presented in Fig. 4 over anatomical data. This superimposition is presented as a set of (R/L, A/P) planes, since in 3D sagittal acquisitions susceptibility-induced distortions could occur along the (R/L) and (A/P) directions.

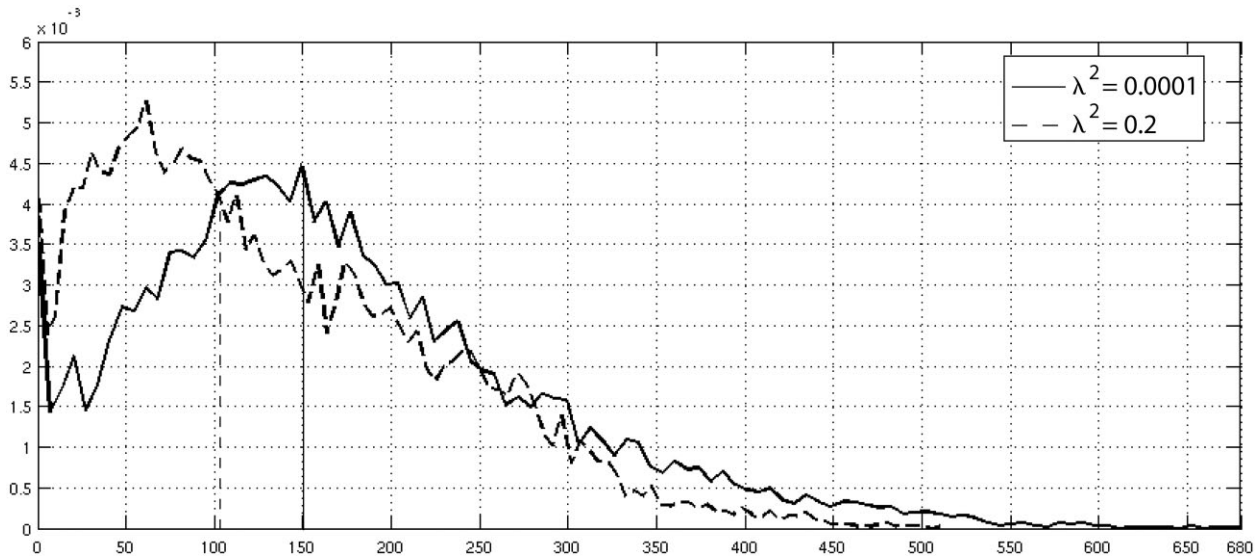


Figure 6. Distributions of temporal SNR values in the voxels of the volume of interest, for subject 1, for two different values of the regularization parameter, $\lambda^2 = 10^{-4}$ (dotted line) and $\lambda^2 = 10^{-2}$ (full line).

were not normally distributed in numerous voxels. Nevertheless, the application of the band-rejection filter made such distributions nearly Gaussian so that SNR could be calculated using the chosen definition. Figure 6 presents the distributions of SNR values in the whole volume, for the smallest and highest regularization parameters (λ^2) applied. These gamma-shaped histograms illustrate the global SNR improvement brought by regularization. Median SNR values, computed from the whole brain, are reported in Table 1 as a function of λ^2 . In agreement with (20,21), regularization increases the temporal stability of parallel EVI data. Moreover, SNR values are very similar for the two subjects and relatively high in spatially smoothed time series.

Geometry factor maps have been computed using the following expression, derived from the geometry factor definition (31), for each voxel ρ of the reconstructed volume:

$$g_{\rho}^{\lambda^2} = \sqrt{[(S^H S + \lambda^2 \cdot Id)^{-1}]_{\rho\rho} \cdot [(S^H S)_{\rho\rho}]}$$

where S is the matrix of the complex coil sensitivities measured in the voxels superimposed in one voxel of the undersampled volume (16). The average, median, and maximum values of the geometry factor experimentally measured are highly similar for the two subjects and decrease to moderate values as λ^2 increases, as

Table 1
Median SNR as a Function of the Regularization Factor.

λ^2	Subject 1		Subject 2	
	before smoothing	after smoothing	before smoothing	after smoothing
0,0001	45	104	51	115
0,01	51	113	56	122
0,04	60	129	63	135
0,1	69	142	69	146
0,2	77	151	75	154

illustrated in Table 2. These values indicate that parallel reconstruction is feasible in the chosen geometry and justifies the SNR improvement observed when regularization is applied. The impact of regularization on the geometry factor is discussed in more detail in Ref. (31).

Activation Detection

In the two subjects, activation in response to the first presentation of the sentences was found along the superior temporal gyri and sulci, and for all λ^2 settings. In all cases, cluster level P -values were inferior to 10^{-4} after family-wise error correction for multiple comparisons. A representative activation map is displayed in Fig. 7 (top), superimposed over anatomical data, for subject 1. In Fig. 7 the presented results were computed from parallel EVI time series reconstructed with $\lambda^2 = 0.2$. The highest SNR results are presented after having checked that no ill-localized activations appear at this λ^2 value. In response to the fourth presentation, the extent of the activating area was reduced (data not shown), as observed previously (27).

In parallel EPI fMRI acquisitions, regularization of parallel reconstruction generally increases the functional contrast-to-noise ratio (CNR), through a noise reduction larger than the contrast reduction (20). This increase in CNR mechanically results in an increased sensitivity to the blood oxygenation level-dependent (BOLD) contrast (20,21). This effect is also observed in parallel EVI. For different values of λ^2 , median t -scores were computed from the 200 most activated voxels in the statistical maps corresponding to the first presentation of the sentences. As illustrated in Fig. 8a, median t -scores increase when λ^2 is increased, as foretold by the SNR increase. Nevertheless, the increase slows down at high λ^2 , as observed in Ref. (21). Besides, if λ^2 is further increased, the regularization condition becomes predominant over the accuracy of the reconstruction, and the reconstructed EVI volumes display

Table 2
Average, Median and Maximum Geometry Factor as a Function of the Regularization Factor

λ^2	Subject 1			Subject 2		
	average g	median g	max g	average g	median g	max g
0,0001	2,53	2,81	4,65	2,47	2,64	5,1
0,01	2,3	2,55	3,84	2,26	2,44	3,94
0,04	1,92	2,09	2,79	1,9	2,06	2,79
0,1	1,57	1,68	2,03	1,56	1,67	2,01
0,2	1,31	1,38	1,56	1,31	1,37	1,56

important artifacts, as illustrated in Fig. 8b. Therefore, the λ^2 value corresponding to the optimal trade-off must be found.

The high acquisition efficiency of parallel EVI acquisition is illustrated in Fig. 7 (bottom), showing HRFs of individual voxels during the four repetitions of a sen-

tence. HRFs were obtained through selective averaging of the experiment time course (32). No temporal smoothing was applied. The BOLD contrast represents around 1% of the baseline signal and a decrease in amplitude and a speeding up of the BOLD response are typically observed with habituation as before (27).

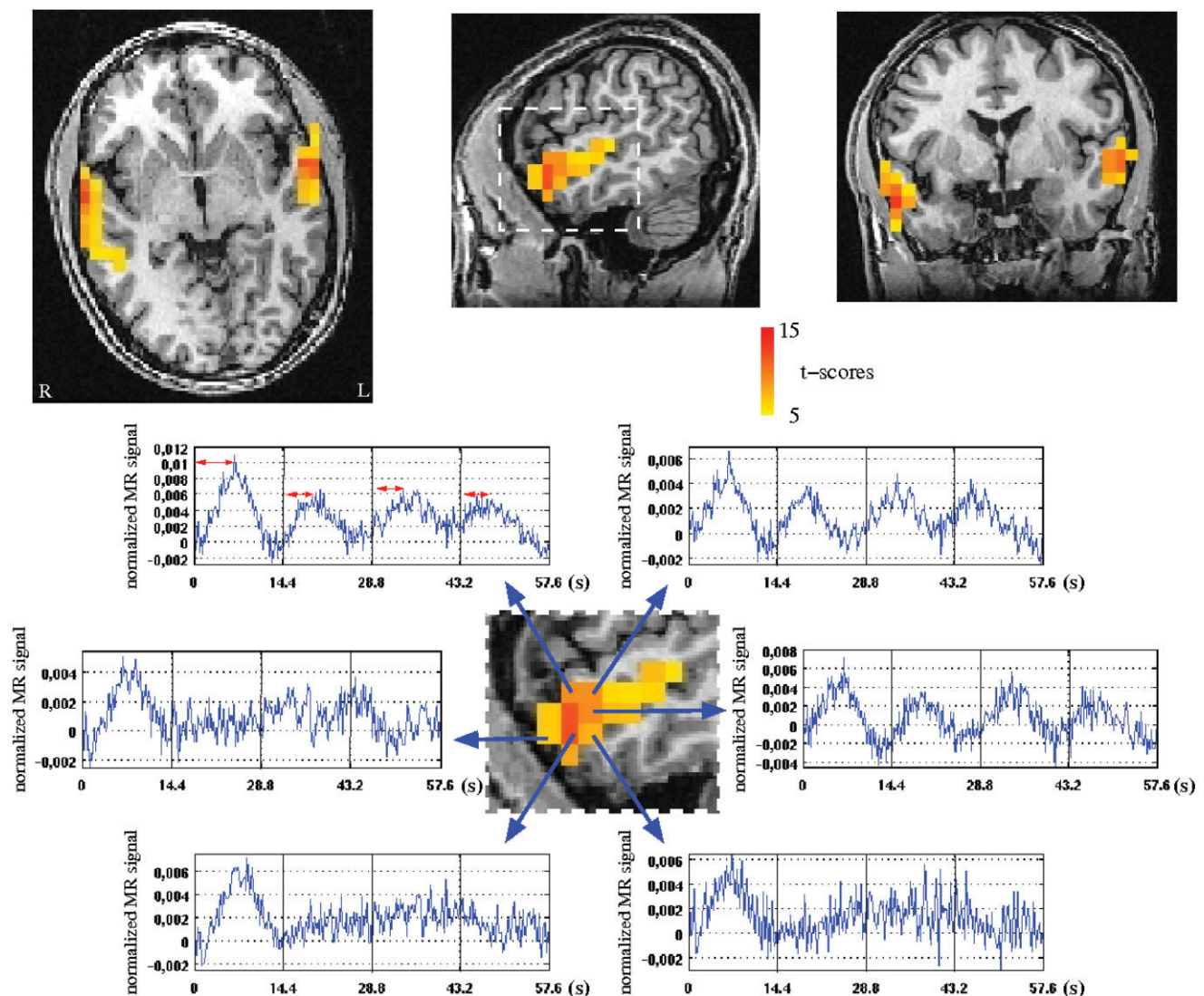
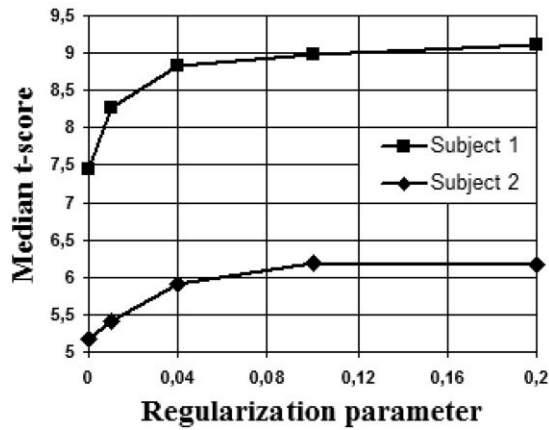
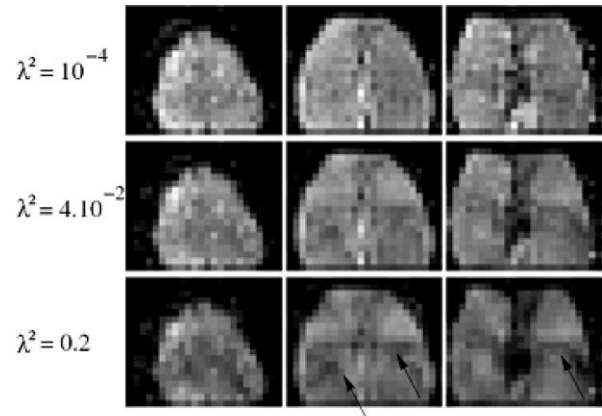


Figure 7. Top: representative activation maps illustrating the areas activated by the first repetition of the sentences, for subject 1 (thresholded at $P < 10^{-4}$, with Family-Wise Error FWE correction for multiple comparisons). Bottom: voxel-wise hemodynamic response for the four presentations of a sentence, obtained through selective averaging of the voxels time courses, after suppression of low-frequency drifts and filtering out of physiological artifacts. Vertical lines materialize the beginning of each presentation of a sentence.



a Statistical scores as a function of λ^2



b Image quality as a function of λ^2

Figure 8. a: Median t -scores computed from the 200 most activated voxels in response to the first presentation of a sentence, as a function of the regularization parameter, for the two subjects. b: Three slices from a parallel EVI brain volume reconstructed with increasing values of the regularization parameter.

Moreover, different habituation behaviors can be distinguished among the voxels eliciting activation in response to the first sentence presentation.

DISCUSSION

To our knowledge, this study presents the first images and fMRI data acquired using parallel EVI. Pioneer studies have demonstrated the high temporal resolution allowed by EVI acquisitions and detection of cerebral activations at relatively high spatial resolution ($3 \times 3 \times 1.5 \text{ mm}^3$) (6). Nevertheless, those studies were limited to anisotropic volumes ($192 \times 96 \times 12 \text{ mm}^3$) (6) due to the important ETD required by EVI. In the present work, parallel imaging allows the reduction of ETD by a factor of 4, which permits covering a larger, nearly isotropic volume of the brain ($120 \times 120 \times 144 \text{ mm}^3$), with a low level of susceptibility-induced distortions and signal losses. Although parallel EVI is currently limited in spatial resolution ($6 \times 6 \times 6 \text{ mm}^3$), it offers a new compromise between FOV and spatial and temporal resolution. Moreover, faster gradient coils and optimized receiver coils with a higher number of acquisition channels will allow improving spatial resolution.

Several methodological difficulties were overcome to perform parallel EVI acquisition of localized volumes. First, a good adequacy between parallel data and sensitivity maps is required for SENSE reconstruction, and is not easily obtained in 3D single-shot imaging. This was achieved through minimization of the ETD in order to reduce distortions and signal losses. Therefore, 2D gradient echo images could be used as sensitivity maps. Second, combining outer volume suppression and parallel imaging requires a very high quality of external signal suppression. Otherwise, a wraparound artifact appears in the reconstructed volume. This efficient signal suppression is allowed by Shinnar-Le Roux designed quadratic phase RF pulses, repeated twice, and combined with spoiler gradients. Third, all imaging parameters were optimized before fMRI acquisitions in order to find the optimal trade-off between short ETD,

acceptable spatial resolution and brain coverage, and adequate SNR. For instance, we studied the impact of the regularization parameter, λ^2 , on functional sensitivity and demonstrated that a trade-off must be found between high SNR and reconstruction accuracy. So far, λ^2 has been empirically set for the whole volume. To avoid this supervised operation and improve the efficiency of the regularization, automatic tuning of λ^2 for each voxel in the folded volume (and each subject) should be considered and an optimal criterion based on functional CNR and spatial reconstruction accuracy should be defined. The tuning could be performed either using the L-curve technique, as before (31), or more efficiently, in the maximum likelihood framework, provided that the penalization remains quadratic (Gaussian likelihood).

After this demonstration of feasibility, several methodological improvements could be made, especially regarding the acquisition strategy and the reconstruction algorithm. Actually, parallel EVI would benefit from a reconstruction algorithm in the k -space domain, like GRAPPA (33), since it would suppress the SENSE-ghost artifact (34). Besides, TGRAPPA (35) takes advantage of the repetitive scanning by temporal shifting the acquired k -space lines in an interleaved manner, which suppress the need for supplementary data. Applying TGRAPPA to parallel EVI would not only reduce the total acquisition time, but also improve image quality by providing sensitivity data with the same geometric distortions as the parallel data and reducing the sensitivity to subject's movement.

In fMRI acquisitions the main requirement is a high temporal SNR (24). In EPI acquisitions, some brain areas always present a low SNR due to distortions and signal losses. Parallel imaging allows reducing the ETD and study these areas with a better SNR (36). Nevertheless, parallel imaging introduces another source of spatial variability of the SNR, because of the spatially inhomogeneous noise in reconstructed images. Thus, spatial maps of the temporal SNR must be considered while interpreting parallel fMRI data and the same dif-

ficuity occurs with parallel EVI. Information about the spatial variations of the SNR is also provided by geometry factor maps. Nevertheless, geometry factors are not reliable estimators of the SNR loss associated with parallel acquisition since they are computed from the sensitivity maps only. For instance, when outer volume suppression is applied, as in the present study, the potential noise magnification due to the "SENSE ghost" is not taken into account. Besides, especially in single-shot acquisitions, the impact of the decrease in TE and ETD allowed by parallel imaging is not considered, and the SNR loss is generally smaller than predicted by the geometry factor (19). Thus, reliable quantitative assessment of the temporal stability is only found in SNR maps.

Increasing the scanning rate and offering 3D single-shot acquisition provides numerous advantages for fMRI studies and could improve the understanding of brain dynamics (37). Indeed, the high acquisition efficiency of parallel EVI allows the extraction of high temporal resolution single-voxel HRF using selective averaging. After this minimal postprocessing, spatial information about the dynamics of the brain response could be extracted and mapped. For example, the large number of samples acquired during the first seconds of the HRF could lead to precise estimation of its initial slope, allowing comparisons of response velocity between different experimental conditions, or voxels. As illustrated in this study, habituation effects, and more generally nonstationary effects, could benefit from parallel EVI, which combines a very high scanning rate and a large coverage of the brain. Moreover, trial-by-trial event-related responses can often be distinguished in activated voxels time courses, which could be interesting for performance-related fMRI studies. High scanning rates are also required in "rest" studies of functional connectivity (38), to avoid aliasing of physiological artifacts over the low frequencies of interest. Finally, the likely reduction of vascular artifacts, which should be investigated in the future, could potentially enhance the specificity of fMRI analysis.

The analysis of parallel EVI data requires further adaptation of activation detection and HRF estimation tools. For instance, the efficiency of the movement correction algorithms should be evaluated in parallel EVI since the mask could hinder the estimation of movement parameters. Moreover, SNR could be further improved by a more efficient correction of the physiological artifacts. Besides, at such a high scanning rate, serial correlation of the noise becomes important and the first-order autoregression model used in SPM2 may not correct efficiently for it (39). Finally, these data will also benefit from more sophisticated estimation tools, incorporating physiological and regional a priori information (2) or performing joint detection and estimation of cerebral responses (40).

In conclusion, parallel EVI was implemented and successfully applied to the detection of brain activations. Combining FOV reduction and 2D parallel acceleration with a reduction factor of 4, 3D single-shot acquisition of a nearly isotropic brain volume could be performed at 1.5T, using a very high scanning rate. Moreover, distortions and signal losses were kept low

since the ETD was similar to the ones used in EPI acquisitions. Tikhonov regularization of parallel reconstruction was applied to improve activation detection and its impact on the sensitivity to the BOLD contrast was studied. Finally, detection of brain activations was demonstrated in a slow event-related auditory paradigm and high temporal resolution, single voxel, hemodynamic response functions were recovered. Combined with advanced estimation tools, parallel EVI should prove useful to measure neural activity timing differences or study the nonlinearities and nonstationarities of the BOLD response.

ACKNOWLEDGMENT

The authors thank Vincent Lebon for valuable assistance in writing the article.

REFERENCES

- Rosen B, Buckner R, Dale A. Event-related functional MRI: past, present, and future. *Proc Natl Acad Sci U S A* 1998;95:773-780.
- Ciuciu P, Poline JB, Marrelec G, Idier J, Pallier C, Benali H. Unsupervised robust nonparametric estimation of the hemodynamic response function for any fMRI experiment. *IEEE Trans Med Imaging* 2003;22:1235-1251.
- Wager T, Vazquez A, Hernandez L, Noll D. Accounting for nonlinear BOLD effects in fMRI: parameter estimates and a model for prediction in rapid event-related studies. *Neuroimage* 2005;25:206-218.
- Mansfield P, Coxon R, Hykin J. Echo-volumar imaging (EVI) of the brain at 3.0 T: first normal volunteer and functional imaging results. *J Comput Assist Tomogr* 1995;19:847-852.
- Yang Y, Mattay V, Weinberger D, Frank J, Duyn J. Localized echo-volume imaging methods for functional MRI. *J Magn Reson Imaging* 1997;7:371-375.
- van der Zwaag W, Francis S, Bowtell R. Improved echo volumar imaging (EVI) for functional MRI. *Magn Reson Med* 2006;56:1320-1327.
- Frahm J, Merboldt KD, Hancic W, Kleinschmidt A, Boecker H. Brain or vein — oxygenation or flow? On signal physiology in functional MRI of human brain activation. *NMR Biomed* 1994;7:45-53.
- Lu H, Golay X, van Zijl P. Intervoxel heterogeneity of event-related functional magnetic resonance imaging responses as a function of T1 weighting. *Neuroimage* 2002;17:943-955.
- Weiger M, Pruessmann M, Boesiger P. 2D SENSE for faster 3D MRI. *MAGMA* 2002;14:10-19.
- Mansfield P. Multi-planar image formation using NMR spin echoes. *J Phys C Solid State Phys* 1977;10:L55-L58.
- Meyer C, Pauly J, Macovski A. Simultaneous spatial and spectral selective excitation. *Magn Reson Med* 1990;15:287-304.
- Le Roux P, Gilles R, McKinnon G, Carlier P. Optimized outer volume suppression for single-shot fast spin-echo cardiac imaging. *J Magn Reson Imaging* 1998;8:1022-1032.
- Bruder H, Fischer H, Reinfelder H, Schmitt F. Image reconstruction for echo planar imaging with nonequidistant k-space sampling. *Magn Reson Med* 1992;23:311-323.
- Ahn C, Cho Z. A new phase correction method in NMR imaging based on autocorrelation and histogram analysis. *IEEE Trans Med Imaging* 1987;6:32-36.
- de Zwart J, van Gelderen P, Kellman P, Duyn J. Reduction of gradient acoustic noise in MRI using SENSE-EPI. *Neuroimage* 2002;16:1151-1155.
- Pruessmann K, Weiger M, Scheidegger M, Boesiger P. SENSE: sensitivity encoding for fast MRI. *Magn Reson Med* 1999;42:952-962.
- Dydak U, Weiger M, Pruessmann KP, Meier D, Boesiger P. Sensitivity-encoded spectroscopic imaging. *Magn Reson Med* 2001;46:713-722.
- Zhao X, Prost RW, Li Z, Li S-J. Reduction of artifacts by optimization of the sensitivity map in sensitivity encoded spectroscopic imaging. *Magn Reson Med* 2005;53:30-34.

19. de Zwart J, van Gelderen P, Kellman P, Duyn J. Application of sensitivity-encoded echoplanar imaging for blood oxygen level-dependent functional brain imaging. *Magn Reson Med* 2002;48:1011–1020.
20. Lin F, Huang TY, Chen NK, et al. Functional MRI using regularized parallel imaging acquisition. *Magn Reson Med* 2005;54:343–353.
21. Ribés A, Poupon C, Rabrait C, Le Bihan D, Lethimonnier F. Tikhonov regularization optimisation for PreLearn: effects on the detection of activation in functional MRI. In: *Proc 15th Annual Meeting ISMRM, Berlin; 2007* (abstract 1757).
22. Tikhonov AN, Arsenin VA. *Solution of ill-posed problems*. New York: Winston-Wiley; 1977:258.
23. King K. SENSE image quality improvement using matrix regularization. In: *Proc 9th Annual Meeting ISMRM, Glasgow; 2001* (abstract 1771).
24. Parrish T, Gitelman D, Labar K, Mesulam MM. Impact of signal-to-noise on functional MRI. *Magn Reson Med* 2000;44:925–932.
25. Goerke U, Möller H, Norris D, Schwarzbauer C. A comparison of signal instability in 2D and 3D EPI resting-state fMRI. *NMR Biomed* 2005;18:534–542.
26. Dietrich O, Reeder S, Reseir SM, Schoenberg S. Influence of parallel imaging and other reconstruction techniques on the measurements of signal to noise ratios. In: *Proc 13th Annual Meeting ISMRM, Miami; 2005* (abstract 158).
27. Dehaene-Lambertz G, Dehaene S, Anton JL, et al. Functional segregation of cortical language areas by sentence repetition. *Hum Brain Mapp* 2006;27:360–371.
28. Holmes A, Josephs O, Buchel C, Friston K. Statistical modelling of low-frequency confounds in fMRI. In: *Proc 3rd Int Conf Funct Mapp Hum Brain, Copenhagen; 1997*:S480.
29. Pruessmann KP, Weiger M, Boesiger P. Sensitivity encoded cardiac MRI. *J Cardiovasc Magn Reson* 2001;3:1–9.
30. Goldfarb J. The SENSE ghost: field-of-view restrictions for SENSE imaging. *J Magn Reson Imaging* 2004;20:1046–1051.
31. Lin F, Kwong K, Belliveau J, Wald L. Parallel imaging reconstruction using automatic regularization. *Magn Reson Med* 2004;51:559–567.
32. Dale A, Buckner R. Selective averaging of rapidly presented individual trials using fMRI. *Hum Brain Mapp* 1997;5:329–340.
33. Griswold MA, Jakob PM, Heidemann RM, et al. Generalized autocalibrating partially parallel acquisitions (GRAPPA). *Magn Reson Med* 2002;47:1202–1210.
34. Griswold MA, Kannengjesser S, Heidemann RM, Wang J, Jakob PM. Field-of-view limitations in parallel imaging. *Magn Reson Med* 2004;52:1118–1126.
35. Breuer FA, Kellman P, Griswold MA, Jakob PM. Dynamic autocalibrated parallel imaging using temporal GRAPPA (TGRAPPA). *Magn Reson Med* 2005;53:981–985.
36. Bellgowan PSF, Bandettini PA, van Gelderen P, Martin A, Bodurka J. Improved BOLD detection in the medial temporal region using parallel imaging and voxel volume reduction. *Neuroimage* 2006;29:1244–1251.
37. Buckner R. The hemodynamic inverse problem: making inferences about neural activity from measured MRI signals. *Proc Natl Acad Sci U S A* 2003;100:2177–2179.
38. Cordes D, Haughton V, Arfanakis K, et al. Frequencies contribution to functional connectivity in the cerebral cortex in “resting state” data. *Am J Neuroradiol* 2001;22:1326–1333.
39. Constable R, Spencer D. Repetition time in echo planar functional MRI. *Magn Reson Med* 2001;46:748–755.
40. Makni S, Ciuciu P, Idier J, Poline JB. Joint detection-estimation of brain activity in functional MRI: a multichannel deconvolution solution. *IEEE Trans Signal Process* 2005;53:3488–3502.